J Mater Sci (2009) 44:5618–5626
DOI 10.1007/s10853-009-3791-2

Pressure effects on elastic and thermodynamic properties of ZrB_2

Hongzhi Fu · Ying Lu · Wenfang Liu · Tao Gao

Received: 31 March 2009 / Accepted: 2 August 2009 / Published online: 15 August 2009

Abstract A theoretical formalism to calculate the single crystal elastic constants for hexagonal crystals from first principle calculations is described. The calculated values compare favorably with recent experimental results. An expression to calculate the bulk modulus along crystallographic axes of single crystals, using elastic constants, has been derived. The calculated linear bulk moduli are found to be in good agreement with the experiments. The shear modulus, Young's modulus, and Poisson's ratio for ideal polycrystalline ZrB_2 are also calculated and compared with corresponding experimental values. The shear anisotropic factors and anisotropy in the linear bulk modulus are obtained from the single crystal elastic constants. The Debye temperature is calculated from the average elastic wave velocity obtained from shear and bulk modulus as well as the integration of elastic wave velocities in different directions of the single crystal. The calculated elastic properties are found to be in good agreement with experimental values when the generalized gradient approximation is used for the exchange and correlation potential. It is found that the elastic constants and the Debye temperature of ZrB_2 increase monotonically and the anisotropies weaken with pressure. The thermal properties including the equation of state, linear compressibility, ductility, and the heat capacity at various pressures and temperatures are estimated.

H. Fu (✉) · Y. Lu
College of Physics and Electronic Information, Luoyang Normal College, Luoyang 471022, People's Republic of China
e-mail: fhzscdx@163.com

W. Liu
College of Chemistry and Chemical Engineering, Luoyang Normal College, Chengdu 610065, People's Republic of China

T. Gao
Institute of Atomic and Molecular Physics, Sichuan University, Chengdu 610065, People's Republic of China

Introduction

Since the discovery of superconductivity at $T_c = 39$ K in MgB_2, the physical properties of the group IV transition metal diborides with simple hexagonal AlB_2-type structure have attracted significant interest. The crystal structure of ZrB_2 is designated as AlB_2-type transition metal diborides with the space group symmetry *P6/mmm*. It is simply a hexagonal lattice in which close packed TM (transition metal) layers are present alternative with graphite-like B layers. Choosing appropriate primitive lattice vectors, the atoms are positioned at TM (0,0,0), B (1/3, 2/3, 1/2), in the unit cell. Traditional applications of such materials are based on their interesting combination of mechanical and transport properties: high melting temperature, high stiffness, and hardness, high thermal and electrical conductivity [1]. The knowledge of such basic characteristics as stiffness and thermal expansion coefficient is obviously important for applications of ZrB_2 as a refractory material, either on its own or as a matrix of a reinforced composite [2]. Naidyuk et al. [3] investigated electron–phonon interaction (EPI) in ZrB_2 by point-contact spectroscopy. Fermi surfaces presented by Shein and Ivanovskii [4] and Rosner et al. [5]. Vajeeston et al. [6] explained the bonding nature with DOS (density of state) and charge density plots. Singh [7] made a theoretical study of EPI in ZrB_2 and TaB_2. Recent advances in GaN optoelectronics have seen ZrB_2 as a promising substrate for epitaxial growth of high quality GaN films [8]. There is very little lattice mismatch between the two materials (0.63%), and their thermal expansion

coefficients are also quite similar [1].The knowledge of elastic and thermal properties of single crystals of ZrB_2 is important for this application. Mahmud et al. [9] and Milman et al. [10] studied the structural, mechanical, and elastic behavior, stiffness and thermal expansion coefficient of ZrB_2 by the ab initio density functional method with the gradient-corrected approximation. The compressibility of a single crystal of ZrB_2 was investigated by Pereira et al. [11].

Elastic properties are also linked thermodynamically to the specific heat, thermal expansion, Debye temperature, melting point, and Grüneisen parameter. Plastic properties of materials are also closely associated with the shear moduli along the slip planes of mobile dislocations. The elastic constants determine the response of the crystal to external forces, as characterized by bulk modulus, shear modulus, Young's modulus, and Poisson's ratio, and obviously play an important part in determining the strength of the materials. Values of elastic constants provide valuable information about the bonding characteristic between adjacent atomic planes and the anisotropic character of the bonding and structural stability. It has also been noticed that there is a correlation between the elastic constants and the melting temperature of a solid. However, previous work [8–11] addressed the structural properties and electronic structure of ZrB_2 at zero pressure. It is known that pressure is an important parameter to tune physical properties, so it attracts us to investigate the elastic and electronic properties of ZrB_2 under pressure. There are few investigations on the properties of ZrB_2 under high pressure and temperature. In this work, we investigate elastic properties and thermal properties of ZrB_2 under pressure and temperature using the first-principles plane-wave method within the generalized gradient approximation.

Computational details

The thermal properties and elastic properties calculations are performed using the pseudo potential plane-wave method within the framework of the density functional theory and implemented through the Cambridge Serial Total Energy Package (CASTEP) Program [12, 13]. This technique has become widely recognized as the method of choice for computational solid structural properties investigations [14]. The thermodynamic properties for ZrB_2 are calculated by the quasi-harmonic Debye model [15]. The exchange correlation energy is described in the generalized gradient approximation (GGA) using the Perdew-Burke-Ernzerhof (PBE) functional [16]. The Zr ($4d^2 5s^2$) and B ($2s^2\ 2p^1$) states are treated as valence electrons. Interactions of electrons with ion cores are presented by the norm conserving pseudo potential for all atoms. In all the high precision calculations, the cutoff energy of the plane-wave basis set is 270 eV for ZrB_2. The special points sampling integration over the Brillouin zone are carried out using the Monkhorst-Pack method with a $9 \times 9 \times 8$ special k-point mesh. The kinetic energy cutoff and mesh of k-points are optimized by performing self-consistent calculations. The self-consistent is considered to be converged when the total energy is 10^{-6} eV/atom. These parameters are sufficient in leading to well-converged total energy and elastic stiffness coefficients calculations.

Results and discussion

Structure properties

The total energy electronic structure calculations are performed over a range of primitive cell volume V from 0.7 V_0 to 1.20 V_0, in which V_0 is the zero pressure equilibrium primitive cell volume. No constraints are imposed on the c/a ratio, i.e., the lattice constants a and c are optimized simultaneously. Since the experimental c/a ratio of ZrB_2 is about 1.120, we calculate a series of different c/a ratios from 1.110 to 1.142, with a step of 0.004. For each volume, we determine the corresponding equilibrium ratio c/a of ZrB_2 by performing total energy calculations on a series of different c/a ratios and minimize the energy as function of c/a. Through these calculations, we can obtain the equilibrium parameters a and c and the corresponding equilibrium ratio c/a of ZrB_2 under arbitrary pressures. The calculated values of $\Delta E(=E-E_0$, E_0 = minimum energy) have been plotted as a function of volume in Fig. 1. We plot ratios a/a_0, c/c_0, and V/V_0, vary with pressure in Fig. 2

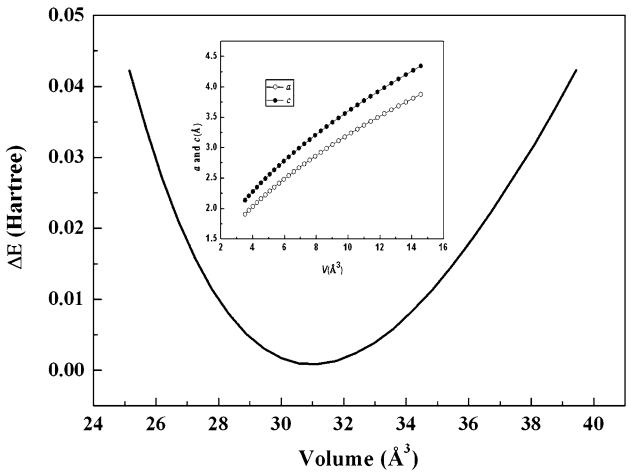

Fig. 1 The energy $\Delta E(=E-E_0)$ as a function of the primitive cell volume of ZrB_2. The *solid curve* is the resulting fit of the Murnaghan equation of state. Inset c/a ratio versus V

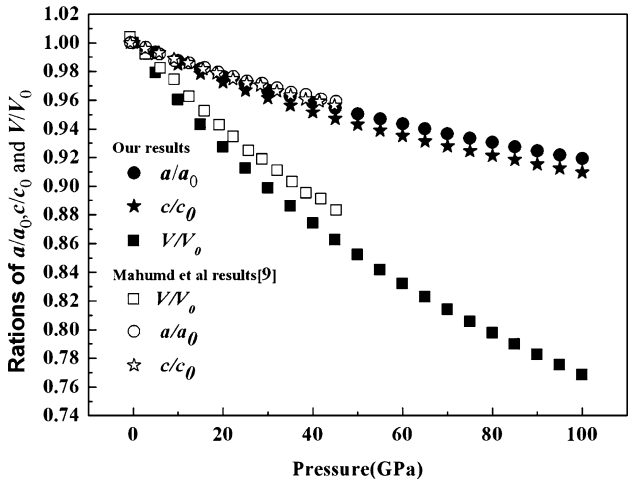

Fig. 2 The normalized volume V/V_0, a/a_0, and c/c_0 as a function of pressure at $T = 0$ where the *dark rectangles*, *circles*, and *asterisks* represent our obtained V/V_0, a/a_0, and c/c_0, respectively, and the blank ones are the results from [9]

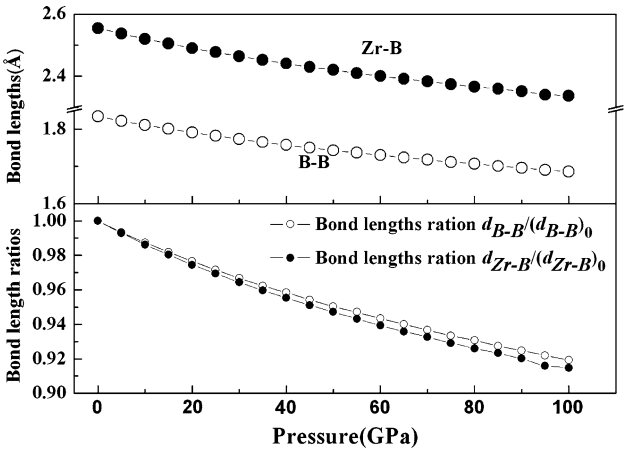

Fig. 3 Variation of the normalized bond length and ratio between the atoms with pressure

together with [9]. It shows that our results are slightly smaller. This may be ascribed to selected different pseudopotential. It is noted that the most stable structure of the ZrB_2 corresponds to the axial ratio $c/a = 1.120$, where $a = 3.1768$ Å, $c = 3.5590$ Å, and equilibrium lattice parameters are listed in Table 1, together with other theoretical [4, 6, 9] and experimental [17–19] data. The zero pressure bulk modulus B_0 and the derivative $B_0'$of the bulk modulus with respect to pressure are obtained from the Birch–Murnaghan equation of state (EOS) [20], and are also shown in Table 1. It is clear that our results are in good agreement with the experimental data [11].

We notice in Fig. 1 that, when pressure increases, the equilibrium ratio c/a ranges from 1.1156 at 20 GPa to 1.1088 at 100 GPa, i.e., decreases by about 0.6%; the compression along the c-axis is much larger than that along the a-axis in the basal plane. The changes of Zr–B and B–B bond distances with the applied pressures are plotted in Fig. 3. This result is important since to a first approximation the vibrational frequencies are dependent on bond distances. As expected experimentally and theoretically, the Zr–B and B–B bond lengths decrease with pressure. Figure 3 indicates that the bond length ratios $d_{Zr-B}/d_{(Zr-B)0}$ become steeper than $d_{B-B}/d_{(B-B)0}$ as pressure increases, indicating that the direction along Zr–B is compressed more difficult. These results agree with Zr–B bonds that determine the lattice parameter c. Moreover, the atoms in the interlayers become closer, and the interactions between them become stronger; contraction of Zr–B and B–B distances under pressure results in the change of bonding anisotropy of ZrB_2 structure. The interlayer linear compressibility $(\mathrm{d}\ln c/\mathrm{d}p = 0.001\ 36\ \mathrm{GPa}^{-1})$ is about 1.28 times larger than that in the basal plane $(\mathrm{d}\ln a/\mathrm{d}\ln p = 0.001\ 06\ \mathrm{GPa}^{-1})$, in which B–B bonds are covalent.

Elastic properties

To calculate the elastic constants under pressure, we have applied the non-volume-conserving method. The complete elastic constant tensor was determined from calculations of the stresses induced by small deformations of the

Table 1 Calculated structure parameters of ZrB_2 compared with the experimental and theoretical results at 0 GPa and 0 K

	a (Å)	c (Å)	c/a	V (Å^3)	B_0 (GPa)	B'	r_{Zr-B}	r_{B-B}
Present	3.1768	3.5590	1.120	31.11	355	4.2	2.55	1.83
Reference [9]	3.1832	3.5464	1.114	31.12	–	–	2.554	1.8378
Reference [6]	3.197	3.561	1.114	31.52	–	–	2.564	1.846
Reference [4]	3.1693	3.5313	1.114	30.72	–	–	–	–
Exp [17]	3.170	3.532	1.114	30.74	–	–	–	–
Exp [18]	3.165	3.547	1.120	30.77	–	–	–	–
Exp [19]	3.168	3.523	1.112	–	–	–	–	–
Exp [11]	–	–	–	–	317	–	–	–
Exp [1]	–	–	–	–	245	–	–	–

equilibrium primitive cell, and thus the elastic constants c_{ijkl} are determined as [21]

$$c_{ijkl} = \left(\frac{\partial \sigma_{ij}(x)}{\partial e_{kl}}\right)_X \quad (1)$$

where σ_{ij} and e_{kl} are the applied stress and Eulerian strain tensors, and X and x are the coordinates before and after the deformation. For the isotropic stress, the elastic constants are defined as [21–23]

$$c_{ijkl} = C_{ijkl} + \frac{P}{2}\left(2\delta_{ij}\delta_{kl} - \delta_{il}\delta_{jk} - \delta_{ik}\delta_{jl}\right) \quad (2)$$

$$C_{ijkl} = \left(\frac{1}{V(x)}\frac{\partial^2 E(x)}{\partial e_{ij}\partial e_{kl}}\right)_X \quad (3)$$

where C_{ijkl} are the second-order derivatives with respect to the infinitesimal strain. For hexagonal crystals, there are five independent elastic constants. In Table 2, we list the elastic constants of ZrB_2 at 0 K and 0 GPa. It is shown that our results are consistent with the experimental data [1] and other theoretical data [9]. The mechanical anisotropy of ZrB_2 can be calculated using the bulk moduli along the a and c axes, B_a and B_c, respectively, defined as [24]

$$B_a = a\frac{dP}{da} = \frac{\Lambda}{2+\alpha}, \quad (4)$$

$$B_c = c\frac{dP}{dc} = \frac{B_a}{\alpha}, \quad (5)$$

$$\Lambda = 2(C_{11} + C_{12}) + 4C_{13}\alpha + C_{33}\alpha^2, \quad (6)$$

$$\alpha = \frac{C_{11} + C_{12} - 2C_{13}}{C_{33} - C_{13}}. \quad (7)$$

The calculated B_a and B_c at zero pressure are also presented in Table 2, together with results of others. The ratio B_a/B_c of ZrB_2 is 1.20 (1.43 for NbB_2 [24, 25], 1.54 for TiB_2 [26], 1.42 for VB_2 [9], 0.98 [9], and 1.22 [1] for ZrB_2), which is in agreement with the experiment value of 1.22 presented by Okamoto et al. The ratio B_a/B_c of ZrB_2 is smaller than NbB_2, TiB_2, and VB_2, indicating the stronger chemical bonding for ZrB_2. The bulk moduli B_a and B_c are also presented in Fig. 4. The ratio of B_a/B_c has a trend of gradual decline as the pressure increases. It is shown that the mechanical behavior of ZrB_2 under zero pressure is of anisotropy. With the applied pressure increasing, the anisotropy will gradually weaken.

Table 2 Elastic constants C_{ij} (GPa) and the bulk moduli B_a and B_c (GPa) at 0 GPa and 0 K

	C_{11}	C_{12}	C_{13}	C_{33}	C_{44}	B_a	B_c
Present ZrB_2	534	55	110	418	244	720	602
Reference [9] VB_2	699	146	109	552	167	999	706
Reference [9] ZrB_2	596	48	169	482	240	809	828
Reference [23, 24] NbB_2	517	95	120	528	122	797	557
Exp [1] ZrB_2	568	57	121	436	248	772	635
Exp [25] TiB_2	660	48	93	432	260	851	553

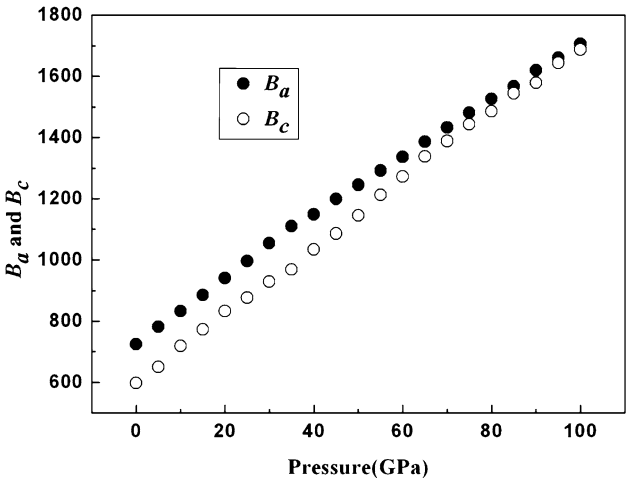

Fig. 4 Variation of the bulk modulus B_a and B_c along the a- and c-axes with pressure

The obtained values of C_{11}, C_{12}, C_{13}, C_{33}, and C_{44} at zero temperature versus pressure (up to 100 GPa) are shown in Fig. 5. We found that the five independent elastic constants increase monotonically with pressure. C_{11} and C_{33} vary rapidly as pressure increases, and C_{44} becomes moderate as well as C_{13}. However, C_{12} increases comparatively slowly with pressure. Unfortunately, there are no experimental and theoretical data to compare our elastic constants under pressure. If this structure is stable, the five independent elastic constants should satisfy the well-known Born stability criteria [27], i.e.,

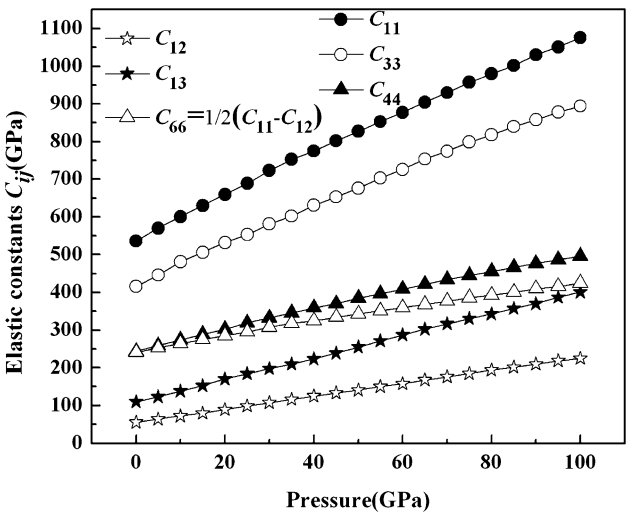

Fig. 5 The elastic constants C_{ij} of ZrB_2 as a function of pressure

$$C_{12} > 0,\ C_{33} > 0,\ C_{66} = (C_{11} - C_{12})/2 > 0,\ C_{44} > 0, \tag{8}$$

and

$$(C_{11} + C_{12})C_{33} - 2C_{13}^2 > 0. \tag{9}$$

It can be seen that our calculated elastic constants C_{ij} satisfy the Born stability criteria. This suggests that the hexagonal phase of ZrB_2 is mechanically stable and predicts that there is not a transition phase when the pressure is under 100 GPa.

The Voigt [28] and Reuss [29] assumptions result in the theoretical maximum and minimum values of the isotropic elastic modulus, respectively. For hexagonal ZrB_2, the Voigt (B_V) and Reuss (B_R) bulk moduli are given by

$$B_V = \frac{1}{9}[2(C_{11} + C_{12}) + C_{33} + 4C_{13}], \tag{10}$$

$$B_R = \frac{(C_{11} + C_{12})C_{33} - 2C_{13}^2}{C_{11} + C_{12} + 2C_{33} - 4C_{13}}. \tag{11}$$

Similarly, the upper and the lower bounds for the shear modulus of polycrystalline ZrB_2 aggregate according to Voigt and Reuss approximations are given by

$$G_V = \frac{1}{30}(C_{11} + C_{12} + 2C_{33} - 4C_{13} + 12C_{44} + 12C_{66}) \tag{12}$$

$$G_R = \frac{5}{2}\frac{\left[(C_{11} + C_{12})C_{33} - 2C_{13}^2)\right]^2 C_{44}C_{66}}{3B_V C_{44}C_{66} + \left[(C_{11} + C_{12})C_{33} - 2C_{13}^2)\right]^2 (C_{44} + C_{66})} \tag{13}$$

where $C_{66} = \frac{1}{2}(C_{11} - C_{12})$.

The arithmetic average of the Voigt and the Reuss bounds is called the Voigt–Reuss–Hill (VRH) average [30] and is commonly used to estimate elastic moduli of polycrystals. The VRH averages for shear modulus (G) and bulk modulus (B) are

$$G = \frac{G_R + G_V}{2},\ B = \frac{B_R + B_V}{2}. \tag{14}$$

The polycrystalline elastic modulus (E) and the Poisson ratio (σ) are then computed from these values using the following relationship [30]:

$$E = \frac{9BG}{3B + G},\ \sigma = \frac{3B - 2G}{2(3B + G)}. \tag{15}$$

It is suggested that the bulk modulus, B, can be used as a measure to describe the average atomic bond strength because it has a strong correlation with the cohesive energy or bonding energy of atoms in crystals [31]. The hardness of materials can be related to their elastic moduli, such as the Yong's modulus, E, and the shear modulus, G [32]. Although the relationships between hardness and the moduli are not identical for different materials, the general trend is, the larger the moduli, the harder the materials. Table 3 lists the calculated polycrystalline elastic modulus, bulk modulus, and the Poisson ratio of ZrB_2 in this study. Therefore, elevating pressure can increase the materials hardness.

The investigation of the elastic properties can be completed by providing the Poisson's ratio, which quantifies the stability of the crystal against shear. The ratio can formally takes values between -1 and 0.5, which corresponds, respectively, to the lower limit where the material does not change its shape, and to the upper limit when the volume remains unchanged. All the calculated Poisson's ratios in Table 3 are close to the value of 0.15 at lower pressure, and vary to the value of 0.25 at higher pressure which means the central interatomic forces under higher pressure [33].

Elastic anisotropies and brittleness

Most of the crystals exhibit elastic anisotropies of varying degree and there have been different ways to represent the elastic anisotropy of crystals. The compression and the shear anisotropic factors provide measures of the degrees of anisotropy in atomic bonding in different crystallographic planes. For a transversely isotropic material (hexagonal), the anisotropies in compressibility and in shear are given by [34]

$$A_{comp} = \frac{S_{33} + 2S_{13}}{S_{11} + S_{12} + S_{13}},\ A_{shear} = \frac{2C_{44}}{C_{11} - C_{12}} \tag{16}$$

where S_{ij} are elastic compliance constants.

A value of unity means that the crystal exhibits isotropic properties and values other than unity represent varying degree of anisotropy. Another way of measuring the elastic anisotropy is given by the percentage of anisotropy in the compression and shear [35]. They are defined as

$$A_{comp} = \frac{B_V - B_R}{B_V + B_R} \times 100\%,\ A_{shear} = \frac{G_V - G_R}{G_V + G_R} \times 100\%. \tag{17}$$

These values can range from zero (isotropic) to one representing the maximum anisotropy. The calculated anisotropy values of A_{comp}, A_{shear}, $A_{comp}(\%)$, and $A_{shear}(\%)$ are 1.21, 1.02, 0.21%, and 1.28%, respectively. It can be seen that the anisotropy both in shear and compression is little. We notice that the anisotropy factor A (= C_{11}/C_{33}) is 1.27 for VB_2. The corresponding value for ZrB_2 is 1.29, which is in very good agreement with the observed value of 1.3 [1]. Although this anisotropy factor is by no means sufficient to confirm the anisotropy of the system, our results do indicate a smaller anisotropy than even TiB_2 (1.53) [26]. Of the five elastic constants, the values of C_{12} and C_{13} are notably small, indicating the brittleness of the boride.

Table 3 The shear modulus G (GPa), bulk modulus B (GPa), and Poission ratio σ at various pressures

P (GPa)	B_V	B_R	B_H	G_V	G_R	G_H	G	B	E	σ
0	226	225	225	226	220	223	223	225	504	0.12797
5	245	244	245	239	233	236	236	245	536	0.13492
10	263	262	262	250	243	246	246	262	563	0.14201
15	282	281	282	262	255	258	258	282	594	0.14858
20	299	298	298	273	264	268	268	298	620	0.15398
25	320	319	319	285	275	280	280	319	651	0.16072
30	331	330	331	292	281	286	286	331	667	0.16404
35	354	353	354	305	293	299	299	354	700	0.17008
40	369	368	368	312	300	306	306	368	720	0.17443
45	387	387	387	324	311	318	318	387	749	0.17768
50	404	403	404	333	318	325	325	404	770	0.18232
55	417	417	417	341	325	333	333	417	790	0.1844
60	434	433	434	349	332	341	341	434	810	0.18862
65	448	448	448	357	339	348	348	448	830	0.19144
70	475	475	475	372	352	362	362	475	867	0.19608
75	486	485	486	375	355	365	365	486	876	0.19927
80	505	505	505	386	367	377	377	505	906	0.20146
85	517	516	517	391	369	380	380	517	916	0.20466
90	532	532	532	398	374	386	386	532	933	0.20784
95	545	545	545	403	379	391	391	545	947	0.21075
100	568	568	568	417	390	404	404	568	979	0.2127

Anisotropic parameters (C_{13}/C_{12}, C_{44}/C_{66}, and C_{33}/C_{11}) are plotted in Fig. 6 as a function of pressure. Both the large C_{13}/C_{12} and small C_{33}/C_{11} values indicate that atomic bonding along the a-axis is stronger than that along the c-axis, being consistent with the fact that the crystal structure of ZrB_2 is a layered-type with respect to the c-axis.

Pugh [36] introduced the quotient of bulk to shear modulus (G/B) of polycrystalline phases by considering that the shear modulus G represents the resistance to plastic deformation, while the bulk modulus B represents the resistance to fracture. A high (low) G/B value is associated with brittleness (ductility). The critical value which separates ductile and brittle materials is about 0.57. It is interesting to try to understand the microscopic origin of this empirical parameter. This was recently demonstrated in the study of brittle versus ductile transition in intermetallic compounds from first principles calculations [37]. All the calculated values of the G/B (>0.57) decrease with pressures which means that pressure can improve ductility (Fig. 7).

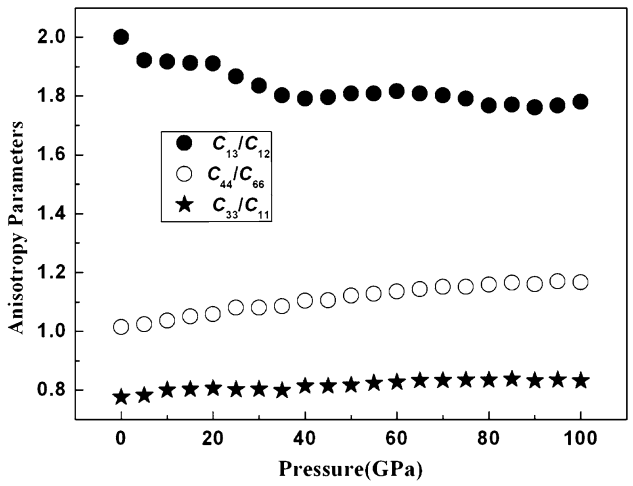

Fig. 6 Anisotropic parameters (C_{13}/C_{12}, C_{44}/C_{66}, and C_{33}/C_{11}) plotted as a function of pressure

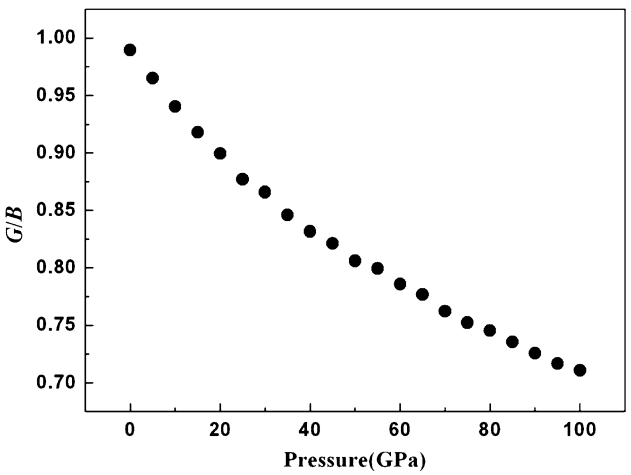

Fig. 7 The calculated ratio of G/B plotted as a function of pressure

Thermodynamic properties

To investigate the thermodynamic properties of ZrB_2, we apply the quasi-harmonic Debye model, in which the non-equilibrium Gibbs function $G^*(V; P,T)$ can be written in the form of [15, 38–41]

$$G^*(V;P,T) = E(V) + PV + A_{\mathrm{Vib}}(\theta(V);T) \tag{18}$$

where $E(V)$ is the total energy per unit cell, PV corresponds to the constant hydrostatic pressure condition, and $A_{\mathrm{Vib}}(\theta(V);T)$ is the vibrational term, which can be written as

$$A_{\mathrm{Vib}}(\theta(V);T) = nKT\left[\frac{9\theta}{8T} + 3\ln\left(1 - e^{-\frac{\theta}{T}}\right) - D\left(\frac{\theta}{T}\right)\right] \tag{19}$$

where n is the number of atoms in unit cell, and the Debye integral $D(\theta/T)$ is defined as [15]

$$D\left(\frac{\theta}{T}\right) = \frac{3}{\left(\frac{\theta}{T}\right)^3}\int_0^{\frac{\theta}{T}} \frac{x^3}{e^x - 1}\mathrm{d}x. \tag{20}$$

The heat capacity C_V and the thermal expansion (α) are expressed as

$$C_V = 3nK\left[4D(\theta/T) - \frac{3\theta/T}{e^{\theta/T} - 1}\right], \tag{21}$$

$$\alpha = \frac{\gamma C_V}{B_T V}, \tag{22}$$

where γ is the Grüneisen parameter defined as

$$\gamma = -\frac{\mathrm{d}\ln\theta(V)}{\mathrm{d}\ln V}. \tag{23}$$

One of the standard methods of calculating the Debye temperature, θ in Eq. 23, is from elastic constant. It is related to an average sound velocity, since the vibrations of the solid are considered as elastic waves in Debye's theory. For ZrB_2 crystal, the Debye temperature can be estimated from the average sound velocity v_m, using the following equation [42]

$$\theta = \frac{h}{k_B}\left(\frac{3nN_A\rho}{4\pi M}\right)^{1/3} v_m \tag{24}$$

where h is Planck's constant, k_B is Boltzmann's constant, N_A is Avogadro's number, M is the molecule mass, ρ is the density, and the average sound velocity v_m is approximately given by [43]

$$v_m = \left[\frac{1}{3}\left(\frac{2}{v_s^3} + \frac{1}{v_P^3}\right)\right]^{-\frac{1}{3}} \tag{25}$$

where v_p and v_s are the longitudinal and transverse elastic wave velocities, respectively, which can be obtained from Navier's equation [42]

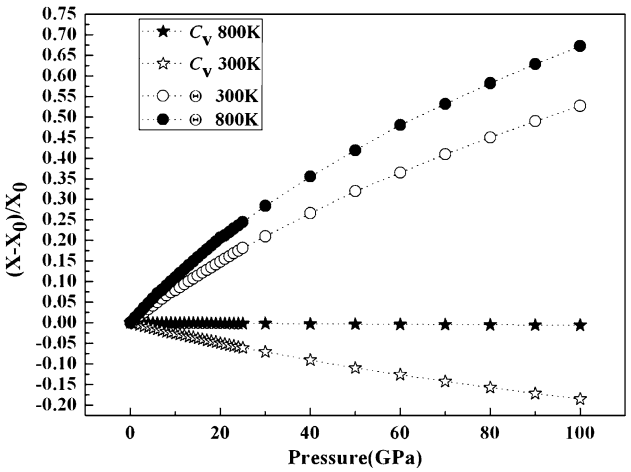

Fig. 8 Variations of thermodynamic parameters X (X Debye temperature or specific heat) with pressure P. They are normalized by $(X - X_0)/X_0$, where X and X_0 are the Debye temperature or heat capacity under any pressure P and zero pressure P_0 at the temperatures of 300 and 800 K

$$v_P = \sqrt{\left(B_s + \frac{4}{3}G\right)/\rho},\ v_s = \sqrt{G/\rho} \tag{26}$$

where G is the shear modulus and B_s is the adiabatic bulk modulus.

In Fig. 8, we show the heat capacity C_V and the Debye temperature θ as a function of pressure P at the temperatures of 300 and 800 K for ZrB_2. It is shown that when the temperature is constant, the Debye temperature θ increases non-linearly with applied pressures, indicating the change of the vibration frequency of atoms under pressure. However, the heat capacity C_V decreases with the applied pressures, in which the increasing pressure might achieve the same result with decreasing temperature on ZrB_2.

The relationship between bulk modulus B and pressure P at different temperature $T = 300$, 900, and 1900 K are shown in Fig. 9. These results indicate that B increases with P at a given temperature and decreases with T at a given pressure.

Linear compressibility

The pressure dependence of the lattice parameter is also related to a combination of elastic constants, and thus we can make use of the linear compressibility k to check the validity of the calculated S_{ij}. In hexagonal crystal, the axial compressibilities k_a and k_c are of the form [44]

$$k_a = -\mathrm{d}\ \ln a/\mathrm{d}P = S_{11} + S_{12} + S_{13},\ k_c = -\mathrm{d}\ \ln c/\mathrm{d}P = S_{13} + S_{23} + S_{33}. \tag{27}$$

Here the k_a and k_c reflect the anisotropy of the linear compressibility. On the other hand, we can determine k_a

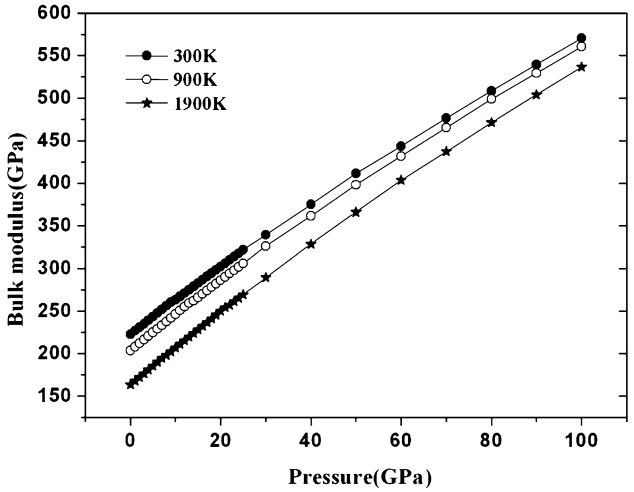

Fig. 9 The relationship of ZrB_2 between bulk modulus B and pressure P at temperatures of 300, 900, and 1900 K, respectively

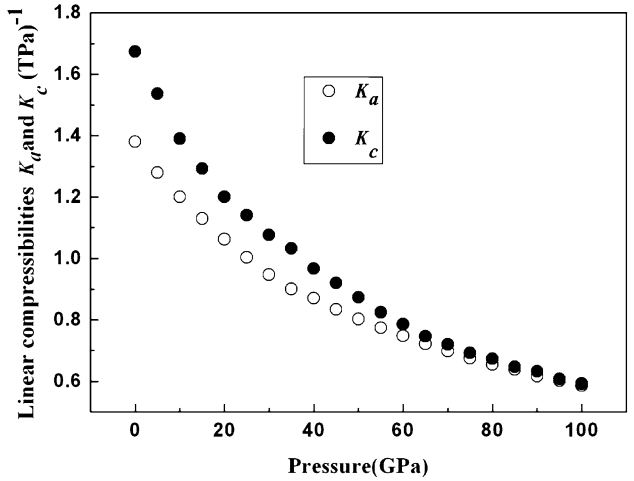

Fig. 10 The linear compresibilities K_a and K_c plotted as a function of pressure

and k_c by fitting a polynomial to the evolution of ln$a$ and ln$c$ at various pressures. Thus we could examine the consistency between the k_a and k_c derived from the strained lattice parameters and those derived from the calculated S_{ij} values. The pressure effects on the axial compressibilities k_a and k_c are shown in Fig. 10. The axial k_a and k_c decrease with increasing pressure but the rate of k_c is little bigger than k_a. This means that the B–B bonds are covalent and stronger than Zr–B bonds. When pressure exceeds 100 GPa, the axial compressibilities k_a and k_c nearly approach the same result (0.6 TPa^{-1}).

Conclusions

In this work, we have used the plane-wave pseudopotential density functional theory within the generalized gradient approximation (GGA) method to perform a set of first principles, self-consistent, total energy calculations to determine the equations of state, and equilibrium structural parameters of ZrB_2in the HCP C32 structure. The calculated lattice constants are in excellent agreement with the experimental data when we use the GGA for the exchange and correlation potential. We have obtained the pressure dependence of structural parameters a, c, c/a, V, and d (the distance of Zr–B, B–B) through performing total energy calculations over a range of the primitive cell volumes. The results are in agreement with other theoretical data. We also calculated the strain energies for five different distortions of ZrB_2 using GGA in the theoretically optimized crystal structure in order to calculate elastic constants. Overall the elastic constants obtained from the GGA calculations are found to be somewhat in better agreement with the experimental values. From the elastic constants, the bulk moduli along the crystallographic axes are calculated and are compared with experimental values. The comparison of directional dependent bulk modulus and Young's modulus obtained from the GGA calculations with experimental results shows that the GGA considerably improves the elastic properties of ZrB_2. Using Hill's approximation, the ideal polycrystalline aggregates bulk modulus, shear modulus, Young's modulus, and Poisson's ratio, are calculated. The Poisson's ratio of ZrB_2 was found to be lower than that of ordinary metals and alloys and this shows clear deviations from central forces in this material. We also discussed the chemical bonding in ZrB_2 through the angular momentum and elastic anisotropy of this material. From the theoretically obtained polycrystalline shear moduli and bulk moduli as well as the average elastic wave velocity over different directions, the Debye temperature was calculated and found to be in good agreement with other theoretical values. The pressure dependences of elastic constants and heat capacity are also obtained. It shows that pressure can improve ductility of ZrB_2. It is found that the elastic constants and the Debye temperature increase monotonically, and the anisotropy and linear compressibility are weakened with pressure.

Acknowledgements This project was supported by the National Natural Science Foundation of China under grant No. 40804034, and by the Natural Science Foundation of the Education Department of Henan province of China under grant No. 2009B590001 and 2007140011, and by Henan Science and Technology Agency of China under grant No. 092102210314.

References

1. Okamoto NL, Kusakari M, Tanaka K, Inui H, Yamaguchi M, Otani S (2003) J Appl Phys 93:88
2. Brown AS (1997) Aerosp Am 35:20

3. Naidyuk YG, Kvitnitskaya OE, Yanson IK, Drechsler SL, Behr G, Otani S (2002) Phys Rev B 66:140301
4. Shein IR, Ivanovskii AL (2001) Preprint cond-mat, 0109445
5. Rosner H, An JM, Pickett WE, Drechsler SL (2002) Phys Rev B 66:024521
6. Vajeeston P, Ravindran P, Ravi C, Asokamani R (2001) Phys Rev B 63:045115
7. Singh PP (2001) Preprint cond-mat. 2003, 0302134 v1; Preprint cond-mat. 2001, 0104580
8. Iwata JI, Siraishi K, Oshiyama A (2003) Phys Status Solidi C 0:2482
9. Mahmud ST, Islam AKMA, Islam FN (2004) J Phys Condens Matter 16:2335
10. Milman V, Winkler B, Probert MIJ (2005) J Phys Condens Matter 17:2333
11. Pereira AS, Perottoni CA, da Jornada JAH, Leger JM, Haines J (2002) J Phys Condens Matter 14:10615
12. Segall MD, Lindan PLD, Probert MJ, Pickard CJ, Hasnip PJ, Clark SJ, Payne MC (2002) J Phys Condens Matter 14:2717
13. Milman V, Winkler B, White JA, Packard CJ, Payne MC, Akhmatskaya EV, Nobes RH (2000) Int J Quantum Chem 77:895
14. Lippens PE, Chadwick AV, Weibel A, Bouchet R, Knauth P (2008) J Phys Chem C 112:43
15. Blanco MA, Francisco E, Luana V (2004) Comput Phys Commun 158:57
16. Perdew JP, Burke K, Ernzerhof M (1996) Phys Rev Lett 77:3865
17. Gasparov VA, Sidorov NS, Zver'kova II, Kulakov MP (2001) JETP Lett 73:532
18. Samsonov GV, Vinitskii I (1976) Refractory compounds. Metallurgia, Moscow (in Russian)
19. Epelbaum VA, Gurevich MA (1958) Zh Fiz Khim 32:2274
20. Murnaghan FD (1994) Proc Natl Acad Sci USA 30:244
21. Karki BB, Ackland GJ, Crain J (1997) J Phys Condens Matter 9:8579
22. Wallace DC (1972) Thermodynamics of crystals. Wiley, New York
23. Barron THK, Klein ML (1965) Proc Phrs Soc 85:523
24. Islam AKMA, Sikder AS, Islam FN (2006) Phys Lett A 350:288
25. Sikder AS, Islam AKMA, Nuruzzaman M, Islam FN (2006) Solid State Commun 137:253
26. Spoor PS, Maynard JD, Pan MJ, Green DJ, Hellmann JR, Tanaka T (1997) Appl Phys Lett 70:1959
27. Born M (1940) Proc Cambridge Philos Soc 36:160
28. Voigt W (1928) Lehrbook, Der Kristallphysik, 2nd edn. Teubner, Leipsig
29. Reuss A (1929) Berechnung der Fliessgrenze von Mischkristallen auf Grund der Plastizitaettsbediengung fuer EinKristalle. Z Angew Math Mech 9:49
30. Hill R (1952) The elastic behavior of a crystalline aggregate. Proc Phys Soc London A 65:349
31. Gschneidner KA (1964) Solid State Phys 16:275
32. Frantsevich IN, Voronor FF, Bokuta SA (1983) Elastic constants and elastic moduli of metals and insulators In: Frantsevich IN (ed) Naukova Dumka, Kiev, p 60
33. Ravindran P, Fast L, Korzhavyi PA, Johansson B (1998) J Appl Phys 84:4891
34. Panda KB, Chandran KSR (2006) Comput Mater Sci 35:134
35. Chung DH, Buessem WR, Vahldiek FW, Mersol SA (eds) (1968) Anisotropy in single crystal refractory compounds. Plenum, New York, p 217
36. Pugh SF (1954) Philos Mag 45:823
37. Cottrel AH (1991) Proceedings of European conference on advanced materials and processes, Cambridge, July 22
38. Francisco E, Recio JM, Blanco MA, Martín Pendás A, Costales A (1998) J Phys Chem A 102:1595
39. Fu HZ, Liu WF, Peng F, Gao T (2009) Physica B 404:41
40. Fu HZ, Hua LD, Feng P, Tao G, Lu CX (2008) Commun Theor Phys 50:1427
41. Fu HZ, Hua LD, Feng P, Tao G, Lu CX (2008) Comput Mater Sci 44:774
42. Anderson OL (1963) J Phys Chem Solids 24:909
43. Poirier JP (2000) Introduction to the physics of the earth's interior. Cambridge University Press, Cambridge, UK
44. Nye JF (1985) Physical properties of crystals: their representation by tensors and matrices. Clarendon, Oxford